Chapter 19
Optical Materials

Yasutaka Suzuki and Jun Kawamata

19.1 Nanosheets and Nanosheet-Based Materials for Optoelectronic Applications

In the last two decades, assemblies of nanosheets or nanosheet-based materials have been fabricated for the development of excellent optical materials. Electrons in nanosheets are confined in the 2D in-plane direction. This anisotropic quantum confinement of electrons is expected to obtain efficient optical responses, especially nonlinear optical (NLO) responses, from nanosheets. Optical materials comprising nanosheet-based hybrid systems have also been developed. In such hybrid materials, nanosheets are used as the host materials of outstanding opto and photofunctional chemical species.

The thickness of a nanosheet is typically smaller than that of an exciton Bohr radius. Thus, a nanosheet is a potential building block of a superlattice so-called quantum well structure. In the quantum wells, the effects of the quantum confinement take place, as described in Sect. 19.4. Owing to the quantum confinement, such materials exhibit prominent and/or unique optoelectronic properties [1–8]. Quantum wells are typically grown by molecular beam epitaxy or chemical vapor deposition with control of the layer thickness down to monolayers. However, the employment of nanosheets makes the fabrication of quantum wells possible without the requirement of a complicated protocol. Actually, several prototypical superlattice structures, using nanosheets as the building blocks, have already been constructed by using the layer-by-layer (LBL) deposition or Langmuir–Blodgett (LB) techniques [9].

Y. Suzuki · J. Kawamata (✉)
Graduate School of Science and Technology for Innovation, Yamaguchi University,
1677-1, Yoshida, Yamaguchi 753-8512, Japan
e-mail: j_kawa@yamaguchi-u.ac.jp

T. Nakato et al. (eds.), *Inorganic Nanosheets and Nanosheet-Based Materials*,
Nanostructure Science and Technology, DOI 10.1007/978-4-431-56496-6_19

Nanosheet-based hybrid materials obtained by intercalation or ion-exchange reactions of opto and photofunctional chemical species exhibit specific optoelectronic functionalities which are not observed in the solution, polymer dispersed, or pure crystalline states, as described in other chapters. In these hybrid materials, the intercalated chemical species are confined in a 2D nanospace. Owing to the confinement, control of the orientation and/or aggregation state of the confined functional chemical species is possible and results in maximizing the functionality. In fact, several hybrid materials, exhibiting an excellent nonlinear optical property [10–18], high luminescence quantum yields [17, 19], and so forth, have been fabricated.

To use the prominent optoelectronic features of nanosheets and nanosheet-based materials as practical devices, the fabrication of low light-scattering solid materials consisting of nanosheet assemblies is an essential requirement. In the first part of this chapter, promising protocols for the fabrication of low light-scattering nanosheet assemblies are described. Then, several nanosheets or nanosheet-based materials exhibiting excellent optical properties will be reviewed.

19.2 Fabrication of Low Light-Scattering Nanosheet Materials

Light scattering from a particle can be categorized as follows. For a particle larger than the wavelength of light, geometric scattering is dominant. This scattering is typically observed in an opaque glass. When a particle size is on the same order as the wavelength of light, Mie scattering occurs, which is the phenomenon causing the white color of clouds. Rayleigh scattering occurs from a particle with a size smaller than the wavelength of light. The white turbidity of milk is a result of Rayleigh scattering of casein micelles with sizes of 20–150 nm. According to the particle size dependence of light scattering, geometric, and Mie scattering are not observed for particles with a size sufficiently smaller than the wavelength of light. In addition, the intensity of the Rayleigh scattering is proportional to the sixth power of the particle size. Therefore, Rayleigh scattering can also be suppressed by decreasing the size of the particle.

Actually, low light-scattering nanosheet materials can be prepared when a small lateral-sized exfoliated nanosheet has been dispersed in water. For example, the transparency of a water dispersion of exfoliated nanosheets with a size smaller than 50 nm is almost the same as that of pure water.

However, for nanosheets in the solid state, light scattering is not always suppressed even when small sized nanosheets are assembled. In a solid nanosheet assembly, a discontinuous point in the refractive index, namely where the particle behaves as an origin of light scattering, occurs at the gap between nanosheets. Therefore, the magnitude of light scattering is strongly related to the size of the gap rather than the size of the nanosheet itself. Considerable light scattering occurs if

the size of the gap is larger than the wavelength of light even when the size of the nanosheet itself is sufficiently smaller than the wavelength of light. Thus, a solid nanosheet assembly in the powder form is a strong light-scattering media. For suppressing such light scattering, decreasing the discontinuity of the refractive index, namely the gap, is important.

Light scattering of solid nanosheet materials can be suppressed for use as optical materials if the size of the discontinuous point of the refractive index can be decreased to be approximately one-tenth that of the wavelength of light. To achieve this, minimization of the size of the gap, namely the preparation of a densely stacked nanosheet assembly, is an effective method. Such an assembly can be constructed through a restacking of the nanosheet followed by exfoliation. Another strategy for minimizing the light scattering from a nanosheet assembly is to fill the gap with an organic compound whose refractive index is almost the same as that of the nanosheet. This strategy is termed index matching.

19.2.1 Restacking Technique

Langmuir–Blodgett (LB)-based and filtration-based techniques can be used with the promising restacking procedures for obtaining low light-scattering nanosheet-based solid materials. For films fabricated by both techniques, exfoliated nanosheets are restacked in a parallel orientation. As a result, the obtained nanosheet assembly possesses 2D anisotropy. Thus, these techniques are useful for the fabrication of nanosheet materials for which anisotropy is an essential requirement. Another feature of the nanosheet assembly obtained by these techniques is that the size of the assembly in the in-plane direction can easily be extended to be in the order of tens of centimeters. This lateral size is sufficient for their practical application as optical materials.

19.2.1.1 Langmuir–Blodgett-Based Technique

The LB technique was originally a fabrication process of a single-layered film of an amphiphilic organic molecule [20]. As already described in detail in Sect. 2.3, a hybrid film consisting of a nanosheet and an organic compound can also be obtained [21, 22] based on the LB technique. Multilayered films can also be constructed to repeat the deposition procedure. During the repetitive deposition, another type of nanosheet can also be inserted by using a trough filled with a dispersion of another type of nanosheet. The thickness of a single-layered LB film is approximately 1 nm and therefore a film of several hundred nanometers can be obtained by several hundred depositions. The LB-based technique is effective to obtain nanosheet-based thin layer films with precise nanosheet orientation or a precisely controlled heterostructure.

The hybrid LB film can be categorized into two groups. The first group is a film consisting of a nanosheet modified by a surfactant [23]. As for the surfactant, a tetraalkylammonium, such as tetramethylammonium (TMA) or tetrabutylammonium (TBA), is typically used. When dispersed in water, part of such an alkylammonium-modified nanosheet can float on water. The floating nanosheets can be collected by mechanical compression of the surface of the subphase to obtain a single-layered nanosheet film. The single-layered nanosheet film can be deposited on a substrate by a vertical dipping or horizontal lifting method. The former film is called a LB film and the latter is a Langmuir–Schaefer film.

Another type of hybrid LB film consists of nanosheets and a functional cationic molecule. For fabricating such films, a water dispersion of an anionic nanosheet exfoliated into a single layer is employed as the subphase. A cationic molecule dissolved in a volatile and nonpolar solvent, such as chloroform, benzene, or so on, is spread onto the subphase. After evaporation of the solvent, the cationic molecule is adsorbed onto a nanosheet near the air–water interface by an ion-exchange reaction. Since the obtained hybrid is hydrophobic, the hybrid floats on water. The resulting floating hybrid is collected and then deposited on a substrate, as is the case for the surfactant-modified nanosheet LB film. In this type of LB film, the molecule spread onto the subphase does not always need to be an amphiphile. The dominant attractive force determining the molecular orientation in the hybrid LB film is an electrostatic interaction between the anionic nanosheet and the cationic molecule. Therefore, oriented molecular alignment can be realized even when a non-amphiphilic molecule is employed as the cationic molecule [24].

An atomic force microscope image of a hybrid LB film, consisting of synthetic saponite (SSA) and tris(4,7-diphenyl-1,10-phenanthroline)ruthenium(II) perchlorate, is shown in Fig. 19.1 [25]. As can be seen from this figure, the gaps between the clay layers are smaller than one-tenth of the wavelength of light and, thus, light scattering from the film is considerably suppressed.

Hybrid LB films thus obtained have been employed for detailed analysis of the properties of a single-layer nanosheet [26], emergence of an electronic property caused by the stacking structure of nanosheet [27] and highly sensitive molecular sensing by using the interlayer space of the stacking structure of the nanosheet [28].

19.2.1.2 Filtration-Based Technique

Nanosheet films with a thickness greater than those obtained by the LB technique can be obtained by filtration of a dispersion of the nanosheet. When the particle size of the nanosheet is larger than the pore size of the filter, the nanosheet will be trapped by the filter. The resulting deposit can be peeled off from the filter to obtain a self-standing film consisting of the nanosheet. This technique can be applied for the fabrication of both a pure nanosheet and a hybrid film. This technique was used for obtaining films where the light-scattering quality of the sample is unimportant, such as for infrared and nucleus magnetic resonance spectroscopies [29].

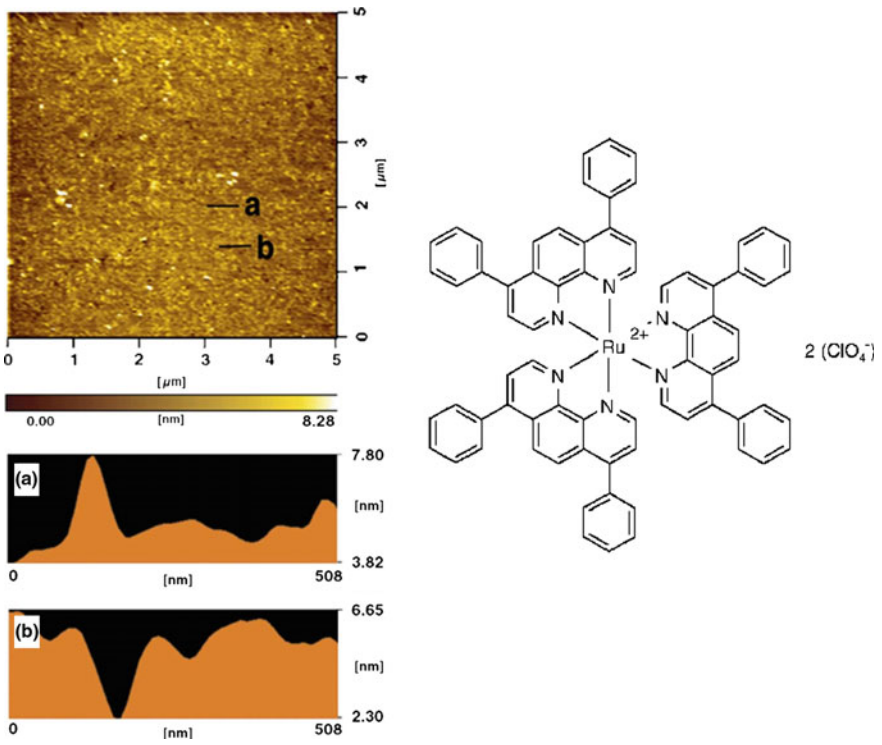

Fig. 19.1 AFM image of a hybrid LB film consisting of synthetic saponite and a ruthenium complex. Reprinted from Ref. [25], Copyright 2006, with permission from Elsevier

A relatively low light-scattering film, suitable for ultraviolet–visible spectroscopic measurements, has been fabricated by Professor S. Takagi's group using the filtration-based technique employing a highly purified synthetic nanosheet [28]. The light scattering of the film fabricated by the filtration-based technique can be further suppressed by careful treatment of the hybrid dispersion [30, 31]. The fabrication protocol of a low light-scattering hybrid film is shown in Fig. 19.2. A cationic molecule dissolved in a water-miscible solvent is added to exfoliate the nanosheet dispersion to obtain a hybrid dispersion. This hybrid dispersion is slowly filtrated using a membrane filter to obtain a low light-scattering film deposited on the membrane filter. The slow filtration also facilitates a parallel stacking of the nanosheets and results in a large anisotropy.

When fabricating a hybrid film with a cationic organic molecule, aggregation (partial stacking) of the hybrid occurs in the dispersion owing to an increase of the hydrophobicity of the nanosheet by hybridization with an organic species [31]. The size of the gap in the film is strongly influenced by the size of the aggregate. Decreasing the particle size of the aggregate results in a decrease in the size of the

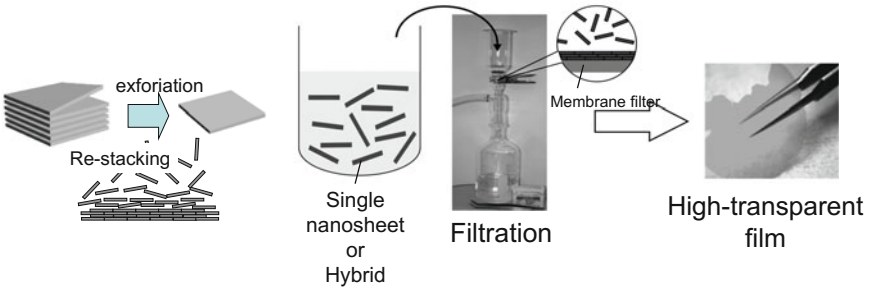

Fig. 19.2 Schematic representation of the fabrication of a hybrid film by the filtration-based technique

gap and thus a low light-scattering film can be obtained. However, the hybrid film cannot be obtained by using smaller-sized particles of the aggregate than that of the pores of the membrane. Therefore, to obtain a low light-scattering hybrid film, control of the aggregate size is crucial. The size of the aggregate is influenced not only by the original particle size of the nanosheet but also by the layer charge, concentration of the nanosheet in the dispersion, hydrophobicity of the employed organic molecule, and the loading level of the hybridized organic molecule. In addition, if an organic solvent is used as a solvent for dissolving the organic molecule, the amount of solvent also influences the size of the aggregate. By optimizing these parameters, a low light-scattering hybrid solid with a haze value of approximately 6% can be obtained. For such a low haze value hybrid film, a laser mode pattern can be retained after passing through the sample. Such materials are suitable as optical devices in terms of the light scattering.

19.2.2 Index Matching by Composition

When two substances with the same refractive index are next to each other, light passes from one to the other without reflection or refraction, and thus, no incoherent light scattering is observed. Such a situation can be realized when the gap between nanosheet particles is filled by a gel or liquid possessing a refractive index close to that of the nanosheet. In optics, such a means is called index matching. Index matching is often used for obtaining optical devices consisting of a heterostructure of different substances.

A schematic representation of an index-matched nanosheet composite is shown in Fig. 19.3. An organic polymer was typically used in early studies as a filler in between the nanosheets [32]. Recently, a small molecular weight molecule, comparable to that of benzene, has also been employed as the filler [33, 34]. Index-matched nanosheet-based materials can be fabricated through the following procedure. The nanosheet is mixed with a polymer or a molecule, which exhibits a

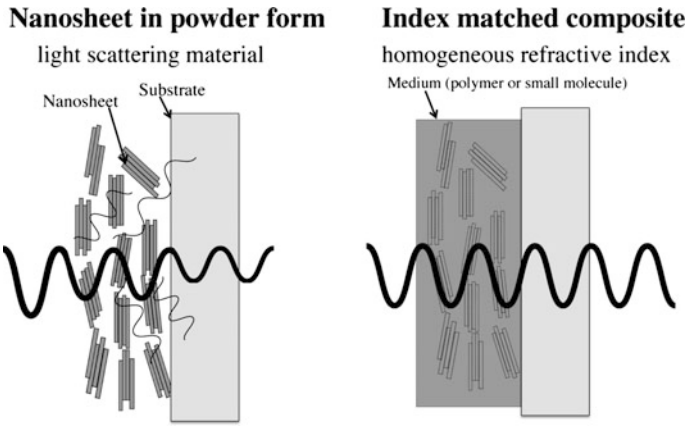

Fig. 19.3 Schematic representation of an index-matched hybrid composite based on a nanosheet. The wave schematically represents the propagation of a laser beam

refractive index close to that of the nanosheet, to obtain a homogeneous gel. The prepared mixed gel is coated on a substrate to obtain a homogeneous composite film. By using this technique, a film, which is thicker than that of a sample fabricated by an LB- or filtration-based technique, can easily be obtained. However, it is difficult to obtain a homogeneous gel by employing functional molecules with a large molecular weight. Most of the functional molecules are hydrophobic. However, nanosheets are typically dispersed in an aqueous media. The preparation of a homogeneous gel consisting of both hydrophilic and hydrophobic components is not easy. Composite films fabricated from an inhomogeneous gel typically exhibit considerable light scattering.

Here, let us demonstrate several index-matched films. A film consisting of SSA and polyacrylic acid is known to exhibit low light-scattering characteristics with a haze value of approximately 6%. The refractive index of SSA has often been considered to be approximately 1.5, though the value has not yet strictly been determined. The refractive index of polyacrylic acid is known to be 1.53, which is comparable with that of SSA. Owing to the similar refractive indices of polyacrylic acid and SSA, the light scattering of a carefully fabricated composite consisting of SSA and polyacrylic acid is very small [32]. A composite employing nanocellulose [35] or poly(*N*-isopropylacrylamide) [36] as the filler has been reported as another example to polyacrylic acid. These composites are expected to be used as a substrate for optoelectronic devices because they are not only low light scattering but also exhibit high flexibility and a gas barrier property.

A homogeneous gel was prepared by mixing sodium hectorite and a small molecule, a fluorescent stilbazolium derivative, in a water and ethanol mixed solvent. A relatively low light-scattering film was obtained by coating the resulting gel to a substrate [34]. According to polarized spectroscopy, each nanosheet was found

to be oriented parallel to the substrate and thus the composite exhibited anisotropy. A low light-scattering composite film employing imidazolium instead of stilbazolium has also been reported [33].

19.3 Nanosheet-Based Optical Material

As briefly described in Sect. 19.1, a nanosheet is expected to possess excellent NLO properties owing to their characteristic form. Therefore, a nanosheet or nanosheet-based optical materials developed to date are mainly NLO materials.

A surface plasmon is an intense nano-sized local electric field that occurs at the surface of metals or semiconductors. This effect is known to induce large NLO responses from a material [37]. Because of the large surface area and nano-sized thickness of the nanosheet, a surface plasmon enhancement and thus a strong NLO response can be effectively induced from semiconducting nanosheets.

Materials possessing quantum well structures have recently received a lot of attention as efficient NLO materials [38–41]. As illustrated in Fig. 19.4, the quantum well is a nanostructure in which a layered semiconductor is sandwiched by another layered substance with a larger energy gap. When the thickness of the sandwiched layer is smaller than the exciton Bohr radius (few to several tens of nm), quantum effects can result. In an appropriately designed quantum well, the exciton can be stabilized owing to the large boundary energy of the exciton. This stable exciton induces a large transition dipole moment, and therefore, a material with a quantum well structure exhibits a large NLO response. A GaAs/AlGaAs quantum well, which is a typical example of an efficient quantum well structured NLO material, was first demonstrated in the 1980 s [42]. Quantum well-structured NLO materials are now widely applied as high-speed optical switches or laser media. A quantum well structure is typically constructed by crystal growth techniques such as molecular beam epitaxy or chemical vapor deposition. Recently, the fabrication of a quantum well has been demonstrated by the stacking of semiconductor nanosheets [9]. It should be noted that a structure can be constructed under ambient pressure and temperature by employing semiconductor nanosheets. Thus, the use of nanosheets has enabled the low-cost construction of a quantum well structure.

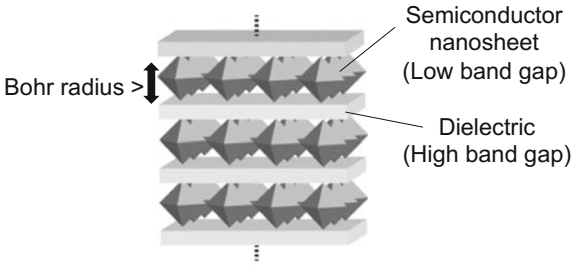

Fig. 19.4 Schematic representation of a nanosheet-based quantum well

Nanosheets have also been used as host materials for excellent opto and photofunctional chemical species. Several organic compounds exhibit considerably larger NLO responses than those of inorganic crystals. However, the growth of organic single crystals required for practical devices, namely sufficient size, lack of defects, and so on, is still not practical [41]. This restricts the application of organic compounds as practical devices. To overcome this problem, several low light-scattering hybrid materials consisting of nanosheets and organic molecules with efficient NLO responses have been fabricated. In such materials, both an excellent NLO response and the requirements for practical devices are realized.

19.3.1 Modulation of Coherent Light by Using a Single-Layer Magnetic Nanosheet [37]

A large magneto-optic response is known to occur by the combination of a magnetic material and a metal nanoparticle owing to the surface plasmon enhancement. A layered magnetic nanosheet, $Ti_{0.8}Co_{0.2}O_2$, was deposited on 50 nm of Au nanoparticles immobilized on a substrate to create a plasmonic nanostructure. This plasmonic nanostructure exhibited an efficient magneto-optical Kerr effect. The magnitude of the Kerr effect was found to be three orders of magnitude greater than that of a single-layered $Ti_{0.8}Co_{0.2}O_2$ nanosheet.

19.3.2 Buildup and Nonlinear Optical Property of Multi-quantum Well Structure

A quantum well structure, consisting of a protonated 4-fluorophenethylamine sandwiched by a semiconductor nanosheet, which is a two-dimensional $(PbI_6)^{4-}$ octahedral sheet was reported by Papagiannouli. The structure of this quantum well was repetitive, alternatively stacking organic and semiconductor layers, namely a multi-quantum well. A third-order NLO response of the multi-quantum well was five orders of magnitude greater than that of quantum dots of PbI_6 [1].

Ishihara reported a $(C_{10}H_{21}NH_3)_2PbI_4$ quantum well that possesses a large boundary energy of the exciton [2]. Owing to the resulting large transition dipole moment, this material is expected to be a good candidate for an NLO material. The $(R–NH_3)_2MX_4$ (R = alkyl chain; M=Pb^{2+}, Sn^{2+}, Ge^{2+}, Cu^{2+}, Ni^{2+}, Mn^{2+}, Fe^{2+}, Co^{2+}, Eu^{2+}; X=Cl^-, Br^-, I^-) type multi-quantum wells were reported as other kinds of nanosheet-based quantum wells [3–8]. They are expected to be used as future electro-optical devices.

19.3.3 Graphene Nanosheet-Based Optical Limiting Materials

Optical limiting devices work as an absorber only when an intense light is irradiated, while it maintains a high transmittance at a low input power. By using this characteristic, protection for optical devices or sensors to the hot spot occurring in a laser system can be realized. A laser with a large output power is typically equipped with an optical limiter. Graphene and graphene oxide nanosheets are known to exhibit an excellent optical limiting property for a pulsed laser [43–45].

Anand reported that the optical limiting property of reduced graphene oxide (rGO) can be increased by increasing the defects of rGO by means of acid post-treatment. Graphene, which is obtained by exfoliation of graphite or graphite oxide in the liquid phase, is known to exhibit an efficient optical limiting property [46, 47]. Graphene with many defects obtained by chemical vapor deposition was also reported to exhibit efficient optical limiting behavior [48, 49].

The optical limiting property of metal nanoparticle modified rGO is further increased compared with that of unmodified rGO. This arises from their charge transfer between the metal and rGO. Modified rGOs with silver [50], copper oxide [51], zinc oxide [52] or all of these metals exhibit efficient optical limiting properties.

19.3.4 Nanosheet–Organic Compound Hybrid Materials for Wavelength Conversion

A π-conjugated molecule, equipped with strong electron donor (D) and strong acceptor (A) groups at both ends of the π-electron system, exhibits a large NLO constant at the molecular level [53]. A typical example of such a molecule is *p*-nitroaniline, which is a so-called D–π–A type molecule. However, most of the D–π–A type molecules crystallized in a centrosymmetric way for the canceling out of their large permanent dipole moment. Given that the centrosymmetric system is second-order NLO forbidden, such centrosymmetric crystals never exhibit second-order NLO effects, even though the NLO constant in the molecular level is large.

Kuroda and coworkers constructed a non-centrosymmetric assembly of *p*-nitroaniline by using the non-centrosymmetric interlayer space of kaolinite, a kind of layered inorganic compound. A schematic representation of the molecular assembly is shown in Fig. 19.5 [10]. The obtained assembly was optical second-harmonic generation (SHG) active, which is a typical second-order NLO effect.

Even when a centrosymmetric interlayer space is employed, an SHG-active hybrid solid is obtained. A hybrid solid obtained by employing SSA and chiral [Ru(1,10-phenanthroline)$_3$]$^{2+}$ was reported to exhibit SHG activity [11]. A model of the

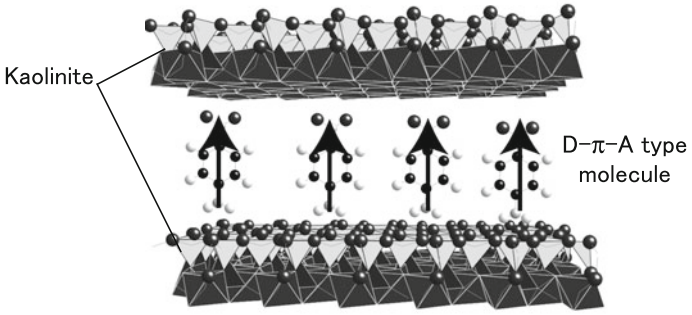

Fig. 19.5 Schematic representation of the interlayer space of the kaolinite–organic hybrid material

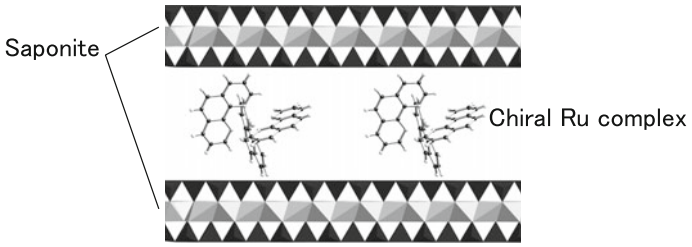

Fig. 19.6 Schematic representation of the interlayer space of a smectite–chiral ruthenium complex hybrid material

molecular alignment of this system is illustrated in Fig. 19.6. In principle, the molecular arrangement of a chiral molecule is non-centrosymmetric. In this system, the nature of the chiral molecule has been ingeniously used.

As for other SHG-active nanosheet–organic molecule hybrids, layered chalcogenophosphates (MPS_3) mixed with stilbazolium derivatives have been reported [12–15]. However, the molecular arrangement and thus the origin of SHG activity in this system is not yet clearly revealed.

19.3.5 Nanosheet–Organic Compound Hybrids with Efficient Two-Photon Absorption Properties

As a strategy for increasing the two-photon absorption (TPA) cross-section (efficiency of TPA) of organic molecules, increasing their transition dipole moment is well established means [54]. For increasing the transition dipole moments of organic molecules, the interlayer space of nanosheets can be used.

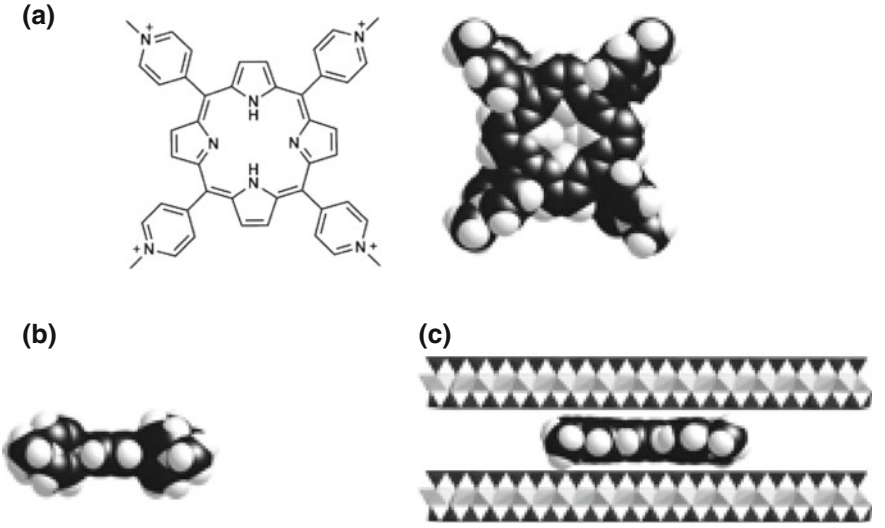

Fig. 19.7 Molecular structure (**a**) and stereo-structures of TMPyP in solution (**b**) and in interlayer space (**c**)

The TPA cross-section of tetrakis(1-methylpyridinium-4-yl)porphyrin (TMPyP; Fig. 19.7a) or 1,4-bis(2,5-dimethoxy-4-{2-[4-(*N*-methyl)pyridinum]ethenyl}-phenyl)butadiyne (MPPBT; Fig. 19.8a) intercalated in a clay mineral were enhanced 13 or 5 times, respectively, compared with those in their solution state [16, 17]. As shown in Fig. 19.7b, in the solution state, the pyridinium groups of TMPyP are not coplanar with respect to the porphyrin ring owing to the steric hindrance. Additionally, in the solution state, the diacetylenic moiety of MPPBT is rotating at room temperature, as can be seen from Fig. 19.8b. However, by confining the interlayer space of a clay mineral, the molecular stereo-structure of these molecules become planar to enhance the π-conjugation, as seen in Figs. 19.7c and 19.8c. As a result, significant enhancement of the TPA cross-sections occur by increasing the transition dipole moments. A direct means for obtaining a molecule with a large transition dipole moment is the design of a molecule with a planar and extended π-electron system. However, the synthesis and treatment of such a molecule is very difficult owing to the strong π–π interaction and thus low solubility. However, the synthesis and treatment of a distorted molecule is relatively easy even when a large π-electron system is involved. Intercalation of distorted molecules into an interlayer space of nanosheets results in a planar molecular stereo-structure. When a molecule with a large but distorted π-electron system is intercalated, the fully π-electron system can be flattened. This results in an extension of the π-electron system and enhanced NLO responses. Design of the NLO materials based on the present strategy is a very effective means for obtaining excellent TPA materials [18].

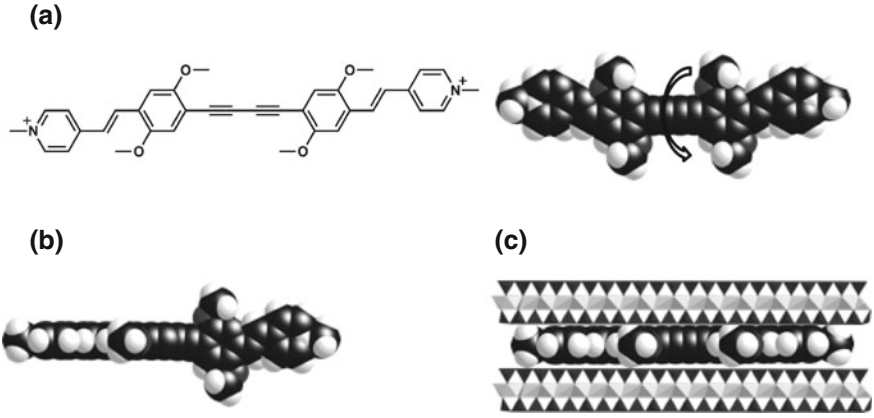

Fig. 19.8 Molecular structure (**a**) and stereo-structures of MPPBT in solution (**b**) and in interlayer space (**c**)

19.4 Conclusions

As discussed in this chapter, various types of nanosheet or nanosheet-based opto-electronic materials can be constructed through soft-chemical processes. The building block, which is the nanosheet itself, possesses various physical properties. The specific characteristics of the nanosheets have ingeniously been used especially for fabricating nanosheet-based plasmonic nanostructures or superlattice devices. Nanosheet-based hybrid materials are also promising candidates for future opto-electronic devices. In such hybrid materials, the potential functionalities of confined molecules can be fully withdrawn.

The key process for creating these materials is the stacking of the nanosheets. A suitable method for constructing (stacking) the nanosheet-based optical materials has not yet been fully developed. Especially, exploration of the available methods for the industrial process remains an important issue for using nanosheet-based optical materials for various practical optical applications.

References

1. Papaginnouli I, Maratou E, Koutselas I, Couris S (2014) J Phys Chem C 118:2766–2775
2. Ishihara T, Takahashi J, Goto T (1989) Solid State Commun 69:933–936
3. Kato Y, Ichii D, Ohashi K, Kungita H, Ema K, Tanaka K, Takahashi T, Kondo T (2003) Solid State Commun 128:15–18
4. Zhang S, Audebert P, Wei Y, Lauret JS, Galmiche L, Deleporte E (2011) J Mater Chem 21:466–476
5. Calabrese J, Jones NL, Harlow RL, Herron N, Thorn DL, Wang Y (1991) J Am Chem Soc 113:2328–2330

6. Dammak T, Koubaa M, Boukheddaden K, Bougzhala H, Mlayah A, Abid Y (2009) J Phys Chem 113:19305–19309
7. Papavassiliou GC, Mousdis GA, Koutselas IB (1999) Adv Mater Opt Electron 9:265–271
8. Xu C, Kondo T, Sakakura H, Kumata K, Takahashi Y, Ito R (1991) Solid State Commun 79:245–248
9. Li BW, Osada M, Ozawa TC, Ebina Y, Akatsuka K, Ma R, Funakubo H, Sasaki T (2010) ACS Nano 4:6673–6680
10. Takenawa R, Komori Y, Hayashi S, Kawamata J, Kuroda K (2001) Chem Mater 13:3741–3746
11. Suzuki Y, Matsunaga R, Sato H, Kogure T, Yamagishi A, Kawamata J (2009) Chem Commun 45:6964–6966
12. Lacroix PG, Clement R, Nakatani K, Zyss J, Ledoux I (1994) Science 263:658–660
13. Bénard S, Yu P, Coradin T, Rivière E, Nakatani K, Clément R (1997) Adv Mater 9:981–984
14. Van der Boom ME, Zhu P, Evmenenko G, Malinsky JE, Lin W, Dutta P, Marks TJ (2002) Langmuir 18:3704–3707
15. Cariati E, Macchi R, Roberto D, Ugo R, Galli S, Casati N, Macchi P, Sironi A, Bogani L, Caneschi A, Gatteschi D (2007) J Am Chem Soc 129:9410–9420
16. Suzuki Y, Tenma Y, Nishioka Y, Kamada K, Ohta K, Kawamata J (2011) J Phys Chem C 115:20653–20661
17. Kamada K, Tanamura Y, Ueno K, Ohta K, Misawa H (2007) J Phys Chem C 111:11193–11198
18. Suzuki Y, Tenma Y, Nishioka Y, Kawamata J (2012) Chem Asian J 7:1170–1179
19. Ishida Y, Shimada T, Takagi S (2014) J Phys Chem C 118:20466–20471
20. Petty MC (ed) (1996) Langmuir-Blodgett films an introduction. Cambridge University Press, Cambridge
21. Inukai K, Hotta Y, Taniguchi M, Tomura S, Yamagishi A (1994) J Chem Soc Chem Commun 959
22. Kotov NA, Meldrum FC, Fendler JH, Tombacz E, Dekany I (1994) Langmuir 10:3797–3804
23. Osada M, Sasaki T (2015) Polymer J 47:89–98
24. Higashi T, Yasui R, Tani S, Ogata Y, Yamagushi A, Kawamata J (2006) Clay Sci 12:42–45
25. Kawamata J, Seike R, Higashi T, Inada Y, Sasaki J, Ogata Y, Tani S, Yamagishi A (2006) Coll Surf A 284–285:135–139
26. Kim HJ, Osada M, Ebina Y, Sugimoto W, Tsukagoshi K, Sasaki T (2016) Sci Rep 6:19402
27. Shibata T, Takano H, Ebina Y, Kim DS, Ozawa TC, Sasaki T (2014) J Mater Chem C 2:441–449
28. Sato H, Tamura K, Taniguchi M, Yamagishi A (2010) New J Chem 34:617–622
29. Kuang W, Facey GA, Detellir C, Casal B, Serratosa JM, Ruiz-Hitzky E (2003) Chem Mater 15:4956–4967
30. Suzuki Y, Hirakawa S, Sakamoto Y, Kawamata J, Kamada K, Ohta K (2008) Clay Clay Mineral 56:487–493
31. Kawamata J, Suzuki Y, Tenma Y (2010) Phil Mag 90:2519–2527
32. Ebina T, Mizukami F (2007) Adv Mater 19:2450–2453
33. Kawasaki K, Ebina T, Mizukami F, Tsuda H, Motegi K (2010) Appl Clay Sci 48:111–116
34. Stöter M, Biersack B, Rosenfeldt S, Leitl MJ, Kalo Schobert H R, Yersin H, Ozin GA, Förster S, Breu J (2015) Angew. Chem Int Ed 54:4963–4967
35. Wu CN, Yang Q, Takeuchi M, Saito T, Isogai A (2014) Nanoscale 6:392–399
36. Haraguchi K, Takehisa T, Fan S (2002) Macromolecules 35:10162–10171
37. Osada M, Hajduková-Smídová N, Akatsuka K, Yoguchi S, Sasaki T (2013) J Mater Chem C 1:2520–2524
38. Arakawa Y, Sasaki H (1982) Appl Phys Lett 40:939–941
39. Schultheis L, Sturge MD, Hegarty J (1985) Appl Phys Lett 47:995–997
40. Faist J, Capasso F, Sivco DL, Sirtori C, Hutchinson AL, Cho AY (1994) Science 264:553–556

41. Zhang S, Lanty G, Lauret JS, Deleporte E, Audebert P, Galmiche L (2009) Acta Mater 57:3301–3309
42. Jovanovic VD, Indjin D, Vukmirovic N, Iknic Z, Harrison P, Linfield EH, Page H, Marcadet X, Sirtori C, Worrall C, Beere HE, Ritchie DA (2005) Appl Phys Lett 86:211117
43. Feng M, Zhan H, Chen Y (2010) Appl Phys Lett 96:033107
44. Song W, He C, Dong Y, Zhang W, Gao Y, Wu Y, Chen Z (2015) Phys Chem Chem Phys 17:7149–7157
45. Tan D, Liu X, Dai Y, Ma G, Menuier M, Qiu J (2015) Adv Optical Mater 3:836–841
46. Anand B, Kaniyoor A, Sai SSS, Philip R, Ramaprabhu S (2013) J Mater Chem C 1:2773–2780
47. Ma F, Zhou ZJJ, Liu YT, Zhang YZ, Miao TF, Li ZR (2011) Chem Phys Lett 504:211–215
48. Hernandez Y, Nicolosi V, Lotya M, Blighe FM, Sun Z, De S, McGovern IT, Holland B, Byrne M, Gun'Ko YK, Boland JJ, Niraj P, Duesberg G, Krishnamurthy S, Goodhue R, Hutchison J, Scardaci V, Ferrari A C, Coleman J N (2008) Nat Nanotechnol 3:563–568
49. Murugan AV, Muraliganth T, Manthiram A (2009) Chem Mater 21:5004–5006
50. Kalanoor BS, Bisht PB, Ali SA, Baby TT (2012) Ramaprabhu S (2012). J Opt Soc Am B 29:669–675
51. Anand B, Kaniyoor A, Swain D, Baby TT, Venugopal Rao S, Sai SSS, Ramaprabhu S, Philip R (2014) J Mater Chem C 2:10116–10123
52. Kavitha MK, John H, Gopinath P, Philip R (2013) J Mater Chem C 1:3669–3676
53. Günter P (ed) (2002) Nonlinear Optical Effects and Materials. Springer, Berlin
54. Rumi M, Ehrlich JE, Heikal AS, Perry JW, Barlow S, Hu Z, McCord-Maughon D, Parker TC, Röckel H, Thayumanavan S, Marder SR, Beljonne D, Brédas JL (2000) J Am Chem Soc 122:9500–9510
55. Takagi S, Shimada T, Eguchi M, Yui T, Yoshida H, Tryk DA, Inoue H (2002) Langmuir 18:2265–2272